ORIGINAL SCIENTIFIC PAPER

CROATICA CHEMICA ACTA

Croat. Chem. Acta **2024**, *97*(4), 231–241
Published online: March 24, 2025
DOI: 10.5562/cca4138

HKD 1926

Diamond/Aqueous Electrolyte Interface: Experimental and Theoretical Approaches

Antun Barišić, Danijel Namjesnik, Tomica Hrenar, Tajana Begović*

Department of Chemistry, Faculty of Science, University of Zagreb, Horvatovac 102a, HR-10000 Zagreb, Croatia

* Corresponding author's e-mail address: tajana.chem@pmf.hr

RECEIVED: October 22, 2024 ⋆ REVISED: January 31, 2025 ⋆ ACCEPTED: February 1, 2025

THIS PAPER IS DEDICATED TO THE LATE PROFESSOR TOMISLAV CVITAŠ

Abstract: This study investigates the effects of pH, ionic strength, and temperature on the diamond/aqueous sodium chloride interface. Analysis were performed on both (100) diamond single crystal (flat surfaces) and diamond colloidal particles. While both surfaces types exhibit a similar affinity for potential-determining ions (H^+ and OH^-), distinct differences were observed in their thermodynamic parameters regarding the distribution of H^+ and OH^- ions between the interfacial layer and the bulk solution. Specifically, reactions on flat surfaces were found to be entropically unfavorable and exhibit a low endothermic contribution. In contrast, colloidal particles displayed an opposite trend, although the overall value of Gibbs free energy was comparable to that calculated for flat surfaces.

Additionally, two distinct ion effects were identified when examining the influence of ionic strength: interfacial water layer compression in the case of flat surfaces and asymmetric counterion association for colloids. These effects were determined to be mutually competitive. To obtain this data, we measured the inner surface potential of diamond in an aqueous electrolyte solution for the first time using a diamond single crystal electrode (DSCrE). Furthermore, the microscopic structure of the interfacial layer near the (100) and (111) diamond crystal planes was studied using localized QM/MM molecular dynamics simulations.

Keywords: diamond, ion distribution, electrical interfacial layer, enthalpy of surface reactions, temperature dependency, point of zero charge, isoelectric point.

INTRODUCTION

DIAMOND, the solid form of carbon, is chemically inert and the hardest known material. When a diamond surface is immersed in an aqueous electrolyte solution, diamond generally does not react with water molecules. In most typical aqueous environments, diamond remains intact and does not dissolve. However, water molecules and dissolved species can be attracted to or repelled from the surface, potentially causing reorientation of water quadripoles and influencing the distribution of dissolved substances. The hydrophobicity of diamond depends on its surface termination: H-terminated diamond surfaces exhibit hydrophobic behavior, while OH-terminated diamond surfaces are hydrophilic.[1] Both surface types remain stable in aqueous electrolyte solutions, necessitating energy-intensive methods like plasma techniques or hot-filament setups to transform H-terminated surfaces to OH-terminated ones.[2] Due to their unique surface properties, chemical stability, diamond surfaces are of significant interest in electrochemical applications, providing an ideal platform for investigating interfacial charging mechanisms of inert material in aqueous electrolyte solutions.[3] H-terminated diamond surfaces are particularly valuable in electrochemistry due to their high surface conductivity, which, combined with diamond's inertness makes them suitable for biochemical sensor applications.[4,5]

Previous studies have shown that increase in salt concentration leads to an increase in drain-source current, attributed to specific adsorption of halogen anion on H-terminated diamond surfaces.[6–8] Hartly and coworkers concluded that variations in surface conductivity are primarily influenced by the pH of the solution rather than its ionic strength.[1]

Hydrophobic inert materials, such as diamond, polytetrafluoroethylene (PTFE), and hydrocarbons, are of special interest because they do not chemically react with

water molecules or ions from aqueous electrolyte solutions. The hydrophobic nature of these surfaces repels water dipoles, leading to a more ordered arrangement of interfacial water molecules compared to those in the bulk solution. This alteration in the ordering and distribution of water molecules and ions near the hydrophobic surface results in the formation of an electrical interfacial layer (EIL).[9,10] Research has shown that the electrical permittivity differs between bulk water and the interfacial water layer (IWL) near hydrophobic surfaces, leading to variations in the equilibrium dissociation constant of water molecules in the interfacial layer compared to the bulk solution.[11,12]

Numerous experiments have been conducted to evaluate surface properties and charge distribution at the interfaces of these inert materials with aqueous solution, including measurements of electrokinetic potential,[13–16] surface tension,[17,18] and bubble potential.[19,20] It has been observed that electroneutrality point for all inert hydrophobic interfaces occurs within the pH range between 2 and 4. This suggests that water behaves similarly at these interfaces, with a preferential adsorption of hydroxide ions leading to a negatively charged surface at neutral bulk pH.[21,22] However, these conclusions have been challenged by studies investigating microscopic properties of IWL, which found no hydroxide ions near surfaces of hydrophobic solids. Instead, they reported that computational analyses indicated the presence of hydronium ions in the first layer.[23–25] Vacha et al provided a succinct summary of this ongoing debate.[26]

While several models have been proposed to explain the electrical charging of hydrophobic materials, there is a notable lack of thermodynamic data regarding interfacial water at these surfaces.[12,27] Understanding the entropy changes associated with ion distribution could elucidate many fundamental questions about the mechanisms at play near hydrophobic surfaces. Since entropy changes cannot be measured, the enthalpy contributions to the Gibbs free energy must be assessed instead.[28] The enthalpy of surface reactions can be determined directly through calorimetric experiments or indirectly by analyzing the temperature dependence of certain equilibrium properties. However, the results of these thermodynamic measurements often do not provide straightforward insights into the system of interest. Instead, they reflect the simultaneous processes occurring within the interfacial water layer.[29]

To extract meaningful thermodynamic data, such as information on the distribution of potential determining ions, a suitable thermodynamic model must be employed to accurately describe the system. In our previous research[30] on interfacial water at PTFE surfaces, we proposed a distribution model to characterize the processes at the interface of inert hydrophobic materials and aqueous electrolyte solution. This model is based on the accumulation of hydronium and hydroxide ions at the interface and considers the distribution of H^+ and OH^- ions between the bulk solution (aq) and the interfacial region (≡).[31] In our model H^+ and OH^- ions represent all possible forms of charged water clusters, with charges (+1) and (–1), respectively.[42] The distribution of positively and negatively charged water cluster is as follows:

$$H^+(aq) \rightleftharpoons H^+$$
$$K^\circ(H^+) = \frac{\exp(\Psi_0 F / RT) \cdot x(\equiv H^+)}{a_c(H^+)}; \quad \Delta_r H^\circ(H^+) \tag{1}$$

$$OH^-(aq) \rightleftharpoons OH^-$$
$$K^\circ(OH^-) = \frac{\exp(-\Psi_0 F / RT) \cdot x(\equiv OH^-)}{a_c(OH^-)}; \; \Delta_r H^\circ(OH^-) \tag{2}$$

where $K°(H^+)$ and $K°(OH^-)$ represent the thermodynamic equilibrium constants for the respective reactions. The relative activities of the interfacial H^+ and OH^- ions are expressed as amount (mole) fractions $x(\equiv H^+)$ and $x(\equiv OH^-)$. The inner surface potential, Ψ_0, refers to the electrostatic potential affecting the interfacial H^+ and OH^- ions. The relative activities of the bulk H^+ and OH^- ions ($a_c(\equiv H^+)$ and $a_c(\equiv OH^-)$), are expressed in terms of molar concentrations.

In addition to H+ and OH– ions, counterions distribute between the bulk aqueous electrolyte solution and the IWL in a manner that ensures the total surface charge density is zero, thereby satisfying the electroneutrality condition. The standard reaction enthalpies $\Delta_r H°(H^+)$ and $\Delta_r H°(OH^-)$ provide insights into the interactions occurring within the interfacial region during the corresponding surface reactions.

In the reaction of self-ionization of water, hydronium and hydroxide ions are generated as follows:

$$H_2O(l) \rightleftharpoons H^+(aq) + OH^-(aq)$$
$$K_w^\circ = \frac{a(H^+) \cdot a(OH^-)}{a(H_2O)} \approx a(H^+) \cdot a(OH^-) \quad \Delta_w H^\circ \tag{3}$$

The indirect method for determining reaction enthalpy involves the temperature dependence of equilibrium parameters. A key parameter that provides insights into surface equilibrium is the electroneutrality point, denoted as pH_{eln}. At this point, both surface potential and surface charge density are zero, effectively minimizing the electrostatic contributions to thermodynamic functions, such as Gibbs energy, enthalpy and entropy. In cases of symmetric or negligible counterion association, the electroneutrality point coincidences with the isoelectric point (pH_{iep}) and point of zero charge (pH_{pzc}); leading to the

relationship $pH_{eln} = pH_{iep} = pH_{pzc}$. The isoelectric point can be easily determined using electrokinetic methods, while the point of zero charge can be assessed through potentiometric acid-base titrations or mass titrations. Relationship between pH_{eln} the corresponding equilibrium constants could be derived from Eqs. (1) – (3):

$$pH_{eln} = \frac{1}{2} \lg \frac{K^{\circ}(H^+)}{K^{\circ}(OH^-) \cdot K_w^{\circ}} \quad (4)$$

From the temperature dependence of the electroneutrality point,[30] the enthalpies of surface reactions can be evaluated by applying Hess's law

$$\frac{dpH_{eln}}{d(1/T)} = -\frac{\Delta_r H(H^+) - \Delta_r H(OH^-) - \Delta_w H^{\circ}}{2R \ln 10} \quad (5)$$

It can be demonstrated that the enthalpy change $\Delta_r H°(H^+) - \Delta_r H°(OH^-) - \Delta_w H°$ is linked to the reaction involving the exchange of H^+ and OH^- ions between the interfacial layer and the bulk solution, as well as the ionization of water molecule in the bulk of the aqueous electrolyte solution:

$$2\ H^+(aq) + \equiv OH^- \rightleftharpoons \equiv H^+ + H_2O(l) \quad (6)$$

The ionization of a water, which produces H^+ and OH^- ions, is an endothermic reaction ($\Delta_w H° \approx 56$ kJ mol^{-1}).[32] To determine the enthalpy associating with the exchange of H^+ and OH^- ions between the interfacial layer and the bulk solution, this value must be subtracted, yielding to the overall reaction:

$$\begin{aligned} &H^+(aq) + \equiv OH^- \rightleftharpoons \equiv H^+ + OH^-(aq) \\ &\Delta_r H^{\circ}(\text{overall}) = \Delta_r H^{\circ}(H^+) - \Delta_r H^{\circ}(OH^-) \end{aligned} \quad (7)$$

In this article we present a comprehensive analysis of diamond/aqueous sodium chloride interface, conducted on both flat diamond single crystal and diamond particles. We discuss and compare the effects of pH, ionic strength and temperature. Notably, we measured the inner surface potential of diamond in aqueous electrolyte solution using a diamond single crystal electrode for the first time. We report on the temperature dependence of the isoelectric point and the point of zero charge for the systems studied. The thermodynamic parameters for the distribution of H^+ and OH^- ions between the interfacial layer and the bulk solution were obtained indirectly from the temperature dependence of equilibrium parameters, specifically the measured electroneutrality points. Apart from experimental research, this paper also includes our theoretical research of the diamond/aqueous electrolyte solution interface. To study microscopic structure of above-mentioned interfacial layer we have conducted QM/MM simulations of aqueous electrolyte at varying pH values at H-terminated diamond surface.

MATERIALS AND METHODS

Diamond Single Crystal

A disk-shaped diamond single crystal (diameter d = 1 cm and thickness l = 5 mm) with (100) crystal orientation was used for streaming potential measurements and the construction of a diamond single crystal electrode (DSCrE). The DSCrE facilitated surface potential measurements.[33] The crystal was synthesized using the chemical vapor deposition (CVD) method. To eliminate organic contamination prior to measurements, the crystal was washed with ethanol and Milli-Q water. Scanning electron microscopy (SEM), secondary ion mass spectrometry (SIMS), and X-ray photoelectron spectroscopy (XPS) confirmed that the diamond had an H-terminated surface. The diamond crystal was utilized for both streaming potential and surface potential measurements via the DSCrE.

Streaming potential measurements were conducted using the SurPass apparatus from Anton Paar. The diamond crystal was adhered to a homemade epoxy carrier and was pretreated with an aqueous solution containing 1 mmol dm^{-3} NaCl and NaOH. The aqueous sodium chloride solution (c(NaCl) = 1 mmol dm^{-3}; $pH_0 \approx 11$) was used to create a potential difference within the measuring cell, while NaOH and HCl were used for pH control. The pH was monitored using a glass electrode calibrated at various temperatures with standard buffer solutions (pH_{buff} = 3, 7, 10). The solution was thermostated in a large vessel, and the temperature was continuously monitored both in this vessel and within the streaming potential cell. Measurements were performed at three different temperatures: 10 °C, 25 °C and 40 °C. The gap height in the measuring cell was manually adjusted to approximately 100 µm, and linear flow checks were conducted before each measurement.

The DSCrE was constructed from the same diamond crystal used in the streaming potential measurements. The (100) diamond plate was fixed to a polyacrylate holder, and the signals from the diamond surfaces were transmitted to the measuring instrument via a copper wire affixed to the back surface of the crystal by conductive paint (Leitsilber L 100, Reichelt elektronik GmbH & Co., Germany) which was also used to cover the whole back surface. Electrode potential from the diamond surface was measured relative to an Ag|AgCl|3M KCl reference electrode, while a glass

electrode was used for precise pH measurements. All three electrodes were immersed in the aqueous sodium chloride solution (c(NaCl) = 1 mmol dm^{-3}). A $pH_0 \approx 3$ was achieved by adding HCl (c(HCl)=0.1 mol dm^{-3}), and pH of the solution was further controlled by adding NaOH (c(NaOH) = 0.1 mol dm^{-3}). Before initiating potentiometric titration, the DSCrE was immersed in the aqueous solution for 16 h to allow the electrode potential to stabilize. The measuring system was thermostated at $\vartheta = 25 \pm 0.1$ °C and maintained under an argon atmosphere (Ar 5.0, Messer) during titration. The stirrer was activated only during the addition of HCl or NaOH to prevent any stirring effects on the measured electrode potential.[34] The signal from the diamond surface was recorded using a Metrohm 827 pH meter every 4 seconds. Data were continuously collected via the RS232 DataLogger 2.7 (Eltima Software) in conjunction with a custom MS Excel worksheet, allowing real-time verification of reading stability. Values of the diamond surface potential were calculated from the measured DSCrE potentials under the assumption that the point of zero potential for the diamond (100)/aqueous electrolyte solution interface corresponds to the isoelectric point determined by streaming potential measurements. This assumption is based on electroneutrality conditions.[35] To investigate the influence of ionic strength on the measured inner surface potential, the experiment was repeated with a more concentrated aqueous sodium chloride solution (c(NaCl) = 10 mmol dm^{-3}; $pH_0 \approx 3$).

Diamond Particles

Synthetic diamond particles were obtained from Alfa Aesar, Kandel, Germany. The specific surface area of these particles was determined using the multiple Brunauer, Emmett and Teller (BET) method (Micromeritics, Gemini) with liquid nitrogen. Prior to this measurement, the diamond powders were outgassed at 150 °C for 2 h. The specific surface area was found to be to be 6.0 ± 0.2 m^2 g^{-1}. These diamond particles were utilized in electrophoresis, dynamic light scattering (DLS) experiments and potentiometric mass titrations.

The electrokinetic zeta potential of the diamond particles as a function of pH was derived from the measured electrophoretic mobilities using a 90Plus Brookhaven instrument. Concurrently, the DLS method was employed on the same instrument to determine the hydrodynamic diameter of the diamond particles at various bulk pH values. The initial suspension was prepared by dispersing diamond particles (γ = 0.06 g dm^{-3}) in sodium chloride aqueous solution of varying NaCl concentrations (c(NaCl) = 1 mmol dm^{-3}; 10 mmol dm^{-3}; 100 mmol dm^{-3}; $pH_0 \approx 11$). Electrophoretic mobilities and hydrodynamic diameters were measured as average values of 10 runs.

The potentiometric mass titration method was used to determine the value of point of zero charge for diamond/aqueous electrolyte solution interface. The initial aqueous solution contained 2 mmol dm^{-3} NaCl and was thermostated at 25 °C. Dry diamond particles were then added to the solution, and changes in the bulk pH were measured. Due to the diamond's low specific surface area, the constant pH_∞, which corresponds to pH_{pzc},[36] could not be reached. Instead, the value of pH_{pzc} was confirmed by adding HCl to the initial aqueous solution until $pH_0 \approx pH_\infty$. After confirming pH_{pzc}, the temperature was lowered to 5 °C and gradually increased in steeps of 5 °C until reaching 50 °C.

Computer Simulation

AB INITIO MOLECULAR DYNAMICS

Simulations of *ab initio* molecular dynamics were performed by sampling Cartesian coordinate space using *on-the-fly* calculations of forces in each simulation point and integration with the velocity Verlet algorithm. A solvent box of dimensions 30 × 30 × 80 Å was generated with a density of 1 g cm^{-3} and placed on diamond surfaces (100) and (111). These surfaces were chosen to represent the experimentally investigated one (100) and an additional one (111) for completeness and comparison. Parallel localized type of molecular dynamics was used for the calculation of trajectories where one point in the simulation was divided into several local calculations using batches of 20 water molecules (*inner system*) for which the forces are calculated (and used in the propagation of dynamics), and all water molecules within 5 Å distance from each water molecule in the inner system (*outer system*). These molecules in the outer system served as an external potential for the motion of the molecules in the inner system. All local calculations were calculated simultaneously using the parallelization algorithm that sends each local calculation to a separate processor core thus enabling almost linear parallelization speedup. Periodic boundary conditions were included during the simulations using replication of the complete system for molecules near the side boundary surfaces. This was used in the generation of inner and outer systems, as well as in the propagation of dynamics where in case one molecule goes outside the box - it appears symmetrically on the other side. For the top surface elastic collision with the surface was used for all molecules. The initial temperature for the Maxwell distribution of velocities was set at 298.15 K, and this temperature was kept constant throughout simulations using a velocity scaling algorithm and total of 100 000 steps were calculated after the initial equilibration phase of 1000 steps.

The surfaces (diamond (100) and (111)) were included in all local calculations for molecules of the inner

system positioned near the surface. The forces were calculated using Gaussian 16 with the PM6 method for solvent molecules (inner and outer system) and the UFF method for the surface. PM6 was chosen based on the literature data about comparison with other semi-empirical methods[43,44] although the reparametrized semiempirical hamiltonians could be an even better solution.[45] Parallel implementation of localized *ab initio* molecular dynamics in our own program ***qcc*** was used for all simulations and propagation of dynamics.[46,47]

PROBABILITY DISTRIBUTION ANALYSIS

For solvent (water) probability distribution analysis each simulation box was divided into horizontal slices of 1 Å height. All solvent molecules, whose center of mass lies within the slice, were counted for each simulation point thus contributing to the probability mass function (PMF).[48,49] For each point of molecular dynamics simulation, the time average was calculated from all previous points, and the final results present the average of the complete simulation. PMF is finally presented as the total number of water molecules in the slices depending on the distance from the investigated diamond surface.

RESULTS AND DISCUSSION

Streaming Potential Measurements

The ζ potentials of (100) diamond crystal plate in a 1 mmol dm^{-3} NaCl aqueous solution were determined from measured streaming currents. Figure 1 shows the calculated ζ potential in relation to the bulk pH value of the sodium chloride aqueous solution at three different temperatures.

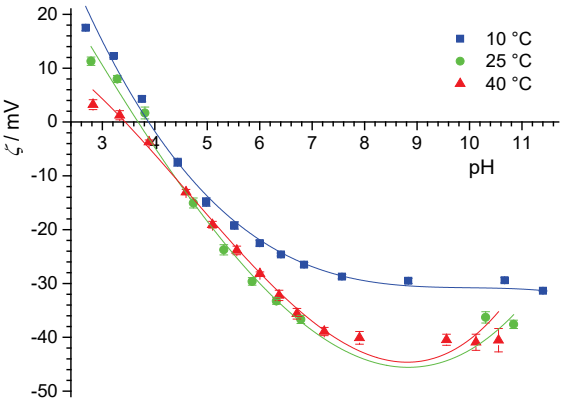

Figure 1. Electrokinetic potential of the diamond (100) crystal plate in a 1 mmol dm^{-3} sodium chloride aqueous solution at various temperatures.

It was found that the ζ potential of the diamond surface depends on both pH of bulk sodium chloride solution and the temperature. Specifically, the isoelectric point of the diamond crystal decreases with increasing temperature: 3.8 ± 0.1 at 10 °C, 3.7 ± 0.1 at 25 °C and 3.5 ± 0.2 at 40 °C. Although the influence of temperature on the measured isoelectric point value is small, it is still measurable. The thermodynamic parameters for the distribution of H^+ and OH^- ions between the bulk solution and the interfacial region were estimated in accordance with Eq. (5). The calculated thermodynamic parameters are presented in Table 1 and will be discussed alongside potentiometric mass titration data at the end of this section.

Single Crystal Electrode Measurements

The construction of a (100) diamond single crystal electrode posed challenges due to low dielectric constant of the diamond crystal. To measure the open circuit potential, a potentiometer with internal resistance of more than 10^{15} Ω was utilized. Before conducting the measurements, the stability and reproducibility of the electrode system were tested. The inner surface potential was calculated from the measured electrode potentials of the diamond single crystal electrode, using the isoelectric point obtained from streaming potential measurement (pH_{iep} (25 °C) = 3.7 ± 0.1) as mentioned above. Figure 2 illustrates the surface potential of the (100) diamond crystal plate in sodium chloride aqueous solution during acidimetric and alkalimetric potentiometric titration at 25 °C. To investigate the impact of ionic strength on the diamond surface potential, experiments were conducted at two different concentrations of sodium chloride.

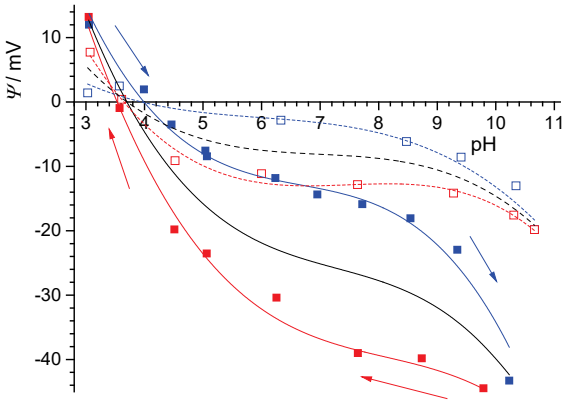

Figure 2. Inner surface potential of the (100) diamond crystal plane, obtained using DSCrE, during alkalimetric (blue symbols: ■, □) and acidimetric (red symbols: ■, □) potentiometric titration in aqueous solution with varying concentration of sodium chloride (■, ■ = 1 mmol dm^{-3}; □, □ = 10 mmol dm^{-3}). Temperature: ϑ = 25 °C.

During alkalimetric potentiometric titration (addition of NaOH) the inner surface potential of the diamond decreases, whereas during acidimetric potentiometric titration (addition of HCl), the inner surface potential increases, indicating that the diamond surface becomes more positive. This pH dependence of the surface potential can be attributed to the distribution of hydronium and hydroxide ions between the inner layer of the IWL and the bulk solution ([Eqs. (1) and (2)]). In the acidic region, the concentration of positively charged hydronium ions is elevated both in the bulk solution and in the interfacial region. The observed hysteresis during acid-base titration suggests different rates and mechanisms for reactions (1) and (2). This hysteresis is particularly pronounced in the neutral pH range between 5 and 8 and diminishes at both lower and higher pH values. It is important to note that within this pH range, the molar concentrations of the potential-determining ions (H^+ and OH^-) are similar, and the hysteresis can be explained by different the diffusion coefficients of hydronium and hydroxide ions near the inert hydrophobic (100) diamond surface. Additionally, hysteresis decreases at higher ionic strength.

An increase of ionic strength results in a significant reduction in the absolute values of the surface potentials (open symbols in Figure 2). This phenomenon can be attributed to a decrease in the thickness of the IWL as the ionic strength of the solution increases. With higher concentrations of counterions, a smaller volume of IWL is required to achieve electroneutrality. Consequently, the slipping plain moves closer to the surface, resulting in a reduction of both the absolute values of the ζ-potential and the inner surface potential, in accordance with Poisson-Boltzmann equation, while the charge density of the potential determining ions and counterions remains unchanged. When the system reaches the isoelectric point, the inner surface potential is also zero, making the ζ-potential at this point are independent of ionic strength. These observations and conclusions are align with the Wnek and Davies theory of surface dissociation for partially hydrated oxides.[37]

Electrophoresis

The electrokinetic ζ-potentials of the diamond particles in sodium chloride aqueous solution during acidimetric potentiometric titration at 25 °C are shown in figure 3. Similar to the the measurements of the inner surface potential of flat diamond, various concentrations of sodium chloride were utilized to investigate the impact of ionic strength on the measured ζ-potentials. Efforts were made to asses the temperature effect on the isoelectric point of the diamond particles through electrophoresis, and to compare these data with those obtained for the flat diamond surface using streaming potential measurements.

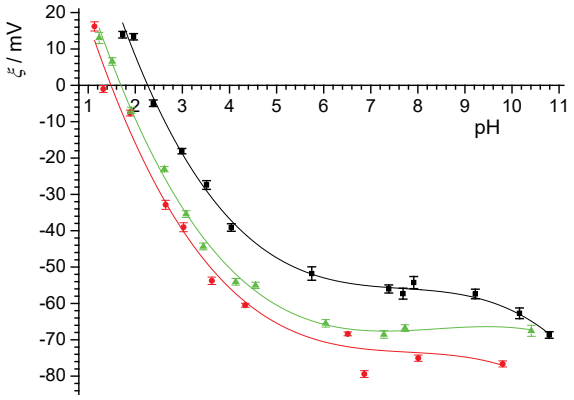

Figure 3. Electrokinetic ζ potential of diamond particles during acidimetric potentiometric titration in an aqueous solution with varying concentrations of sodium chloride (■ = 1 mmol dm^{-3}; ▲ = 10 mmol dm^{-3}; ● = 100 mmol dm^{-3}). Conditions: γ = 0.06 g dm^{-3}; ϑ = 25 °C.

Unfortunately, the measurements conducted at elevated temperatures proved to be unreliable.

The measured electrokinetic ζ-potential values of diamond particles at the lowest sodium chloride concentration (c = 1 mmol dm^{-3}) can be compared to electrokinetic measurements conducted on diamond crystal. The isoelectric point of the diamond particles is shifted toward a more acidic region, with a value pH_{iep} = 2.2 ± 0.1 at 25 °C. It is important to note that during acidimetric potentiometric titration at low sodium chloride concentrations, there is a sharp increase in ionic strength, bellow pH < 3. However, there is still a significant shift in pH_{iep} of diamond particles toward lower pH compared to the pH_{iep} of flat diamond (100) crystal plain. These changes may arise from the distinct structure of the flat diamond (100) crystal plane and the less defined surfaces of the colloid particles.

Our previous studies for metal oxides in aqueous electrolyte solutions provided substantial evidence that interfacial water layer, as well as surface charges and surface potentials, depend on the microscopic structure of solid surfaces.[38,39] The shift in the isoelectric point of diamond particles dispersed in aqueous sodium chloride solution toward lower pH values may result from partial OH surface termination of the diamond. Härtly and coworkers measured the streaming potential of both H-terminated and OH-terminated diamond crystals, concluding that that OH-terminated diamonds exhibited a significantly lower pH_{iep} then their H-terminated counterparts.[1]

The surface properties of both diamond particles and flat diamond crystal surface are influenced by pH and ionic strength. An increase in ionic strength results in shifts of ζ(pH) curves and the isoelectric point of diamond

particles, indicating asymmetric affinities of the counterions (sodium and chloride ions) toward the diamond surface within the interfacial water layer. Specifically, chloride anions show a greater tendency to associate with the diamond particle surface than sodium cations. As the bulk concentration of sodium chloride increases, more chloride ions enter the interfacial water layer then sodium ions, leading to a reduction in the ζ-potential and shifts of the isoelectric point to a more acidic region. The asymmetric counterion association, unlike IWL compression, has a significant impact on the measured pH_{iep} values.

When comparing the ζ-potential values of diamond particles at two higher ionic strengths (c(NaCl) = 10 mmol dm^{-3} and 100 mmol dm^{-3}), the impact of asymmetric counterion association on the measured results diminish. These observations suggest that IWL compression (observed at flat crystal surfaces) and asymmetric counterion association (observed at particle surfaces) are competing effects.

From these measurements, we can draw conclusions about the influence of ionic strength on the IWL. Asymmetric counterion association is more pronounced when the surface area is larger, resulting in a greater IWL volume. As the concentration of counterions increases, more energy is required for them to penetrate the IWL, making the effects of IWL compression effects more significant. The diamond crystal has a smaller surface area exposed to the aqueous solution compared to suspended particles, which results in IWL compression being the dominant effect on the flat diamond crystal. In contrast, the exposed surface of diamond particles is much larger, making asymmetric counterion association the prevailing effect at relatively low sodium chloride concentrations. However, at higher sodium chloride concentrations, the influence of asymmetric counterion association weakens, and IWL compression becomes more prominent.

Dynamic Light Scattering

The hydrodynamic diameter of diamond particles was determined by DLS for two sodium chloride concentrations (Figure 4).

The average hydrodynamic diameter of the diamond particles in the neutral and alkaline pH regions (pH > 5) was found to be 350 ± 22 nm. The value of ζ-potential in this pH region is relatively high (about –50 mV), as shown in Figure 3, it can be assumed that measured hydrodynamic diameter corresponds to non-aggregated diamond particles. With increasing ionic strength in this pH region, the surface charge density and electrokinetic ζ-potential of the diamond particles increase, but the size of the particles remains the same, indicating that aggregation does not occur. Aggregation of the diamond particles appears at pH

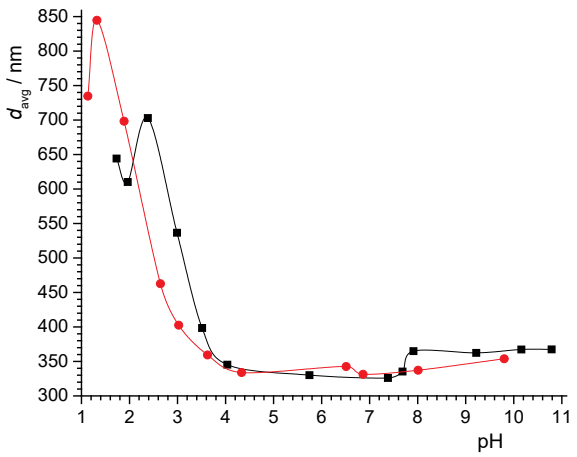

Figure 4. Hydrodynamic diameter of diamond particles during acidimetric potentiometric titration in aqueous solution with different concentration of sodium chloride (■ = 1 mmol dm^{-3}; ● = 100 mmol dm^{-3}). γ = 0.06; ϑ = 25 °C.

values below 4 and reaches its maximum at pH = 2.4 and pH = 1.3, for lower and higher ionic strength, respectively. These values are within the same pH range as the isoelectric points obtained by electrophoresis of the diamond particles. An increase in ionic strength causes larger hydrodynamic diameter of diamond particle aggregates in the isoelectric point region.

Potentiometric Mass Titration

Potentiometric mass titration was conducted by continuous addition of solid diamond particles into sodium chloride aqueous solution. The aim of this measurement is

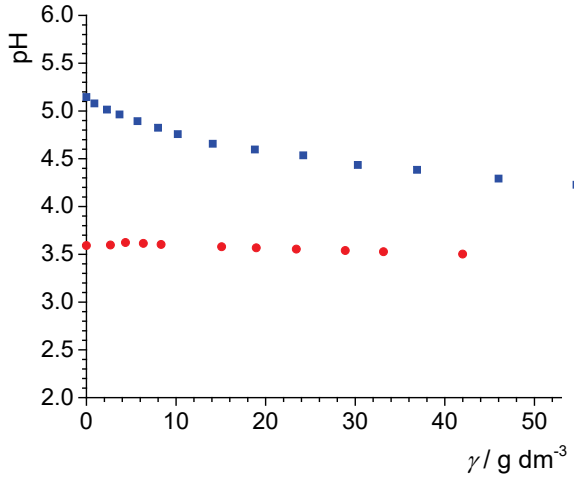

Figure 5. Potentiometric mass titration of colloid diamond particles in 2 mmol dm^{-3} sodium chloride aqueous solution. (■) Pure sodium chloride solution, (●) sodium chloride solution with the addition of HCl. ϑ = 25 °C.

to reach a constant pH value by addition of solid particles, at which one can assume that the obtained pH value represents point of zero potential (PZC) of the system ($pH_\infty \rightarrow pH_{pzc}$). In the case of the diamond particles, the constant pH, pH_∞ could not be reached due to their small surface area (s = 6.0 ± 0.2 $m^2\ g^{-1}$). Therefore, the small amount of HCl was added into the initial sodium chloride solution to adjust the initial pH value closer to the expected pH plateau. The constant pH was reached at mass concentration greater than 10 g L^{-1} and $pH_\infty = pH_{pzc} = 3.5$ value was obtained (Figure 5).

Obtained value of the PZC is at higher pH value than the pH_{iep} of diamond particles obtained via electrophoretic measurements (pH_{iep} = 2.2). As explained earlier, during electrophoretic measurements there is a constant change in ionic strength of the suspension due to the addition of NaOH. During potentiometric mass titration experiment, mass concentration of the diamond particles and the pH of the suspension change, but the ionic strength of the suspension remains the same. To conclude, the observed discrepancy in the measured PZC and IEP value indicates the asymmetric association affinities of counterions towards the diamond surface.

Temperature dependency of the PZC was obtained by varying the temperature of the suspension after potentiometric mass titration (γ = 50 g dm^{-3}). The results are presented in Figure 6, together with the temperature dependency of the isoelectric point of a flat diamond (100) crystal plate measured by means of streaming potential.

The effect of temperature on electroneutrality is the same for the diamond particles and the flat (100) diamond crystal plate. An increase in temperature causes pH_{iep} and

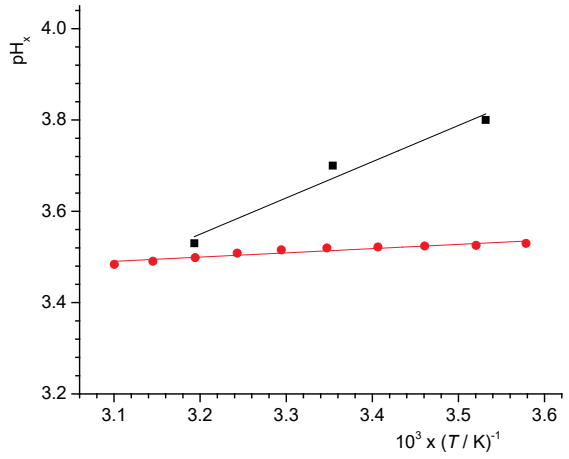

Figure 6. Temperature dependency of (■) pH_{iep} of diamond (100) crystal plate obtained via streaming potential measurements; and (●) pH_{pzc} of colloid diamond particles obtained via potentiometric mass titration.

Table 1. Thermodynamic parameters for hydronium and hydroxide ion distribution between the diamond interface and the bulk of the aqueous sodium chloride solution described by reaction (7).

	slope / K	$\Delta_r G°$(overall) / kJ mol^{-1}	$\Delta_r H°$(overall) / kJ mol^{-1}	$\Delta_r S°$(overall) / kJ mol^{-1}
Diamond crystal	880	38	22	–54
Diamond particles	92.78	40	52	42

pH_{pzc} to decrease. Also, for both systems a linear dependency of the pH(1/T) function can be obtained and in accordance with the Eq. (5), thermodynamic parameters can be obtained. Table 1 shows calculated values of Gibbs energy, enthalpy and entropy for the overall reaction represented by Eq. (7). While the calculated values of Gibbs energy are similar for the flat diamond crystal plate and diamond particles, there is significant difference in calculated enthalpy and entropy. The positive value of Gibbs energy obtained for both diamond surfaces indicates that the reverse reaction, in which hydroxide ions enter the inner layer of the IWL and push hydronium ions into the bulk of the solution, is more favorable. This observation is in agreement with results obtained for inert / aqueous solution interfaces and the conclusion that hydroxide ions more easily accumulate inside the IWL than hydronium ions.[12,20,40] In the case of the diamond crystal, reverse reaction is both enthalpy and entropy driven while in the case of diamond particles it's entirely enthalpy driven with unfavorable entropic contribution. The difference in the obtained thermodynamic parameters between flat plane and the particles could arise from different hydrogen bond structuring around the plains and curvatures, but there is insufficient evidence in this research to support that claim.

Ab Initio Molecular Dynamics

Molecular dynamics simulations using the parallel localized approach where water molecules were divided into *inner system* batches of 20 molecules and *outer system* molecules that serve as an external potential were performed for both diamond surfaces (100) and (111). The outer system was built from the molecules within the 5 Å radius of each inner system molecule ensuring the proper potential description of the forces acting on the inner system molecules. Diamond surfaces (diamond (100) and (111)) were included in all local calculations for molecules of the *inner system* positioned near the surface (Figs. 7 and 8). Collected trajectories were analyzed and the PMF of solvent distribution was calculated in both cases. Global maximum in distribution analysis was at 4 Å for diamond surface (100) (Figure 9) and at 3 Å for diamond surface (111) (Figure 10). One can expect these results because of

the different directions of C–H bonds on the investigated surfaces of diamond. The maximum number of water molecules was similar for both surfaces whereas the distribution curves show two distinct layers near the surfaces with two local maxima in water density for (100) and (111) surfaces. It is clear that approximately after 8 Å distance surface has no additional effect on the water molecule distribution and their behavior starts to be the same as in bulk.

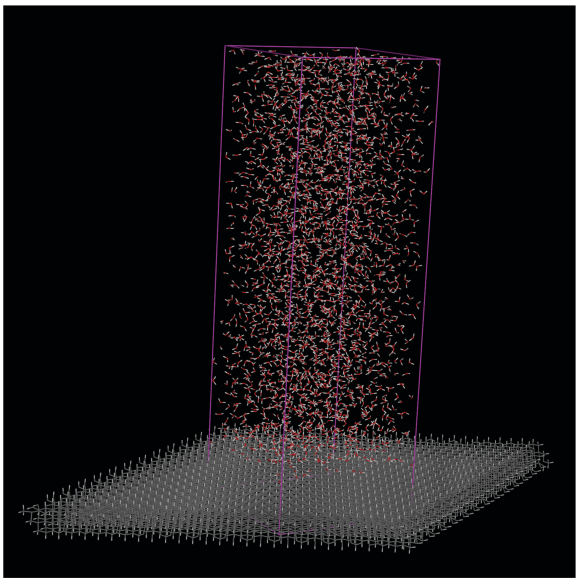

Figure 7. Water box (30 × 30 × 80 Å) placed on the surface of the diamond (111).

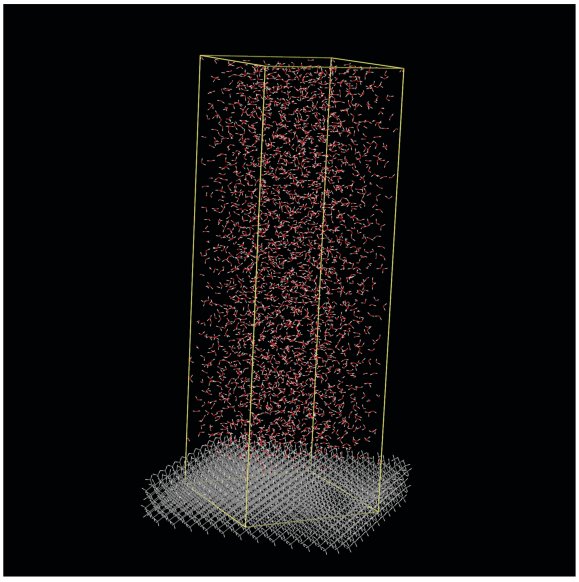

Figure 8. Water box (30 × 30 × 80 Å) placed on the surface of the diamond (100).

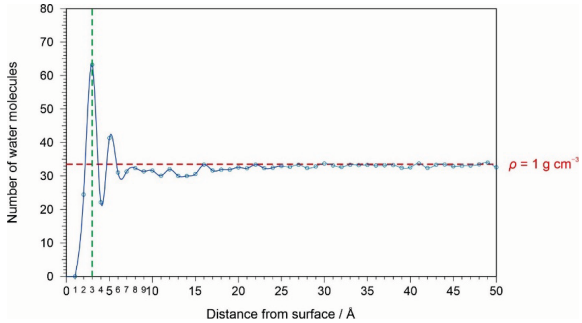

Figure 9. Probability mass function of water distribution in dependence on the distance from the diamond (111) surface.

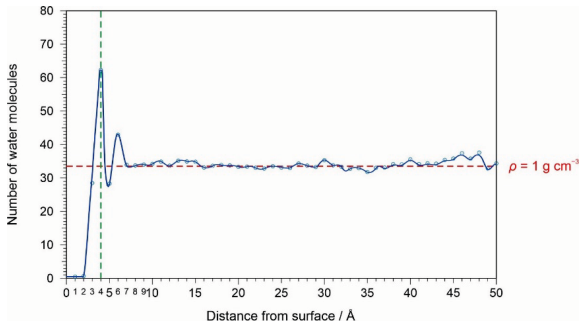

Figure 10. Probability mass function of solvent distribution in dependence on the distance from the diamond (100) surface.

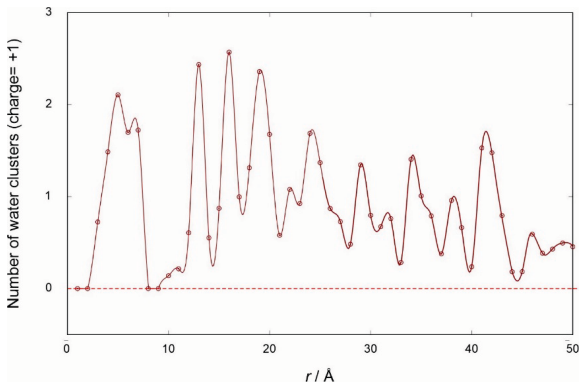

Figure 11. Probability mass function of charged particle distribution in dependence on the distance from the diamond (100) surface.

Simulation performed with the charged water molecules (pH=1.5) on the surfaces of the diamond provided a distribution of charged water clusters (with charge +1) (Figure 11). PMF shows that the first layer of charged water clusters is placed in the range from 3 to 8 Å followed by the charge hole with no charged clusters. From 12 Å further, there is a smooth distribution of charged particles with transition to the constant number of charged particles in the bulk.

CONCLUSION

We have presented a comprehensive analysis of the diamond / aqueous sodium chloride interface conducted on diamond single crystal and diamond particles, coupled with computational QM/MM calculations. The observed pH dependence of the zeta and inner surface potentials indicates that hydronium and hydroxide ions are potential-determining ions for diamond surface.

Thermodynamic parameters for the reactions involving the distribution of H^+ and OH^- ions between the interfacial layer and bulk of the solution were obtained indirectly from the temperature dependency of equilibrium parameters i.e. measured electroneutrality points. A positive value of reaction Gibbs free energy shows that substitution of hydroxide ions with hydronium ions in the inner layer of IWL is an energetically unfavorable reaction. Therefore, a large concentration of hydronium ions is needed for IWL neutralization (low pH value), which is in accordance with other experiments conducted on inert / aqueous solution interfaces.[20,27,30,41] However, a difference was found in the entropic contribution toward free Gibbs energy between measurements conducted on the diamond single crystal and the diamond particles, indicating that surface curvature influences the hydrogen bond network of water molecules surrounding it.

For the first time, the inner surface potential of a diamond was measured in an aqueous electrolyte solution by means of a diamond single crystal electrode. An increase in ionic strength caused a significant reduction in the absolute value of the surface potentials, explained by the reduction in thickness of the IWL due to the increase in the ionic strength of the solution (IWL compression). However, in the case of diamond particles (electrophoresis and DLS measurements), an increase in ionic strength led to a more "classical" effect of asymmetric counterion association being observed. We conclude that two competing effects occur in both types of systems. Asymmetric counterion association is the more dominant effect in the case of larger surface areas and thus larger IWL volumes. But as the concentration of counterions increases, more energy is needed for them to enter IWL, and thus IWL compression effects become more dominant.

Simulations of QM/MM molecular dynamics confirmed the existence of multiple layers near the diamond surfaces (at least two) and provided insight into the microscopic picture of water molecules distribution. Distinct maxima present at 3 Å for (111) surface and at 4 Å for (100) surface show the increased density of the water layer near the surface and the reduced density follower by an additional maximum for both surfaces. As expected, due to the different chemical structures of surfaces, the maximum for (100) surfaces is shifted to 4 Å revealing that there is an additional space of approx. 1 Å between the diamond surface and solvent molecules compared to the (111) surface.

REFERENCES

[1] A. Härtl, J. A. Garrido, S. Nowy, R. Zimmermann, C. Werner, D. Horinek, R. Netz, M. Stutzmann, *J. Am. Chem. Soc.* **2007**, *129*, 1287–1292. https://doi.org/10.1021/ja066543b

[2] F. Maier, M. Riedel, B. Mantel, J. Ristein, L. Ley, *Phys. Rev. Lett.* **2000**, *85*, 3472–3475. https://doi.org/10.1103/PhysRevLett.85.3472

[3] G. M. Swain, A. B. Anderson, J. C. Angus, *MRS Bull.* **1998**, *23*, 56–60. https://doi.org/10.1557/S0883769400029389

[4] M. I. Landstrass, K. V. Ravi, *Appl. Phys. Lett.* **1989**, *55*, 975–977. https://doi.org/10.1063/1.101694

[5] W. Yang, O. Auciello, J. E. Butler, W. Cai, J. A. Carlisle, J. E. Gerbi, D. M. Gruen, T. Knickerbocker, T. L. Lasseter, J. N. Russell, L. M. Smith, R. J. Hamers, *Nat. Mater.* **2002**, *1*, 253–257. https://doi.org/10.1038/nmat779

[6] K.-S. Song, T. Sakai, H. Kanazawa, Y. Araki, H. Umezawa, M. Tachiki, H. Kawarada, *Biosens. Bioelectron.* **2003**, *19*, 137–140. https://doi.org/10.1016/S0956-5663(03)00174-X

[7] H. Kanazawa, K.-S. Song, T. Sakai, Y. Nakamura, H. Umezawa, M. Tachiki, H. Kawarada, *Diam. Relat. Mater.* **2003**, *12*, 618–622. https://doi.org/10.1016/S0925-9635(03)00035-9

[8] T. Sakai, K.-S. Song, H. Kanazawa, Y. Nakamura, H. Umezawa, M. Tachiki, H. Kawarada, *Diam. Relat. Mater.* **2003**, *12*, 1971–1975. https://doi.org/10.1016/S0925-9635(03)00277-2

[9] J. K. Beattie, *Lab Chip* **2006**, 6, 1409. https://doi.org/10.1039/b610537h

[10] V. Tandon, S. K. Bhagavatula, W. C. Nelson, B. J. Kirby, *Electrophoresis* **2008**, *29*, 1092–1101. https://doi.org/10.1002/elps.200700734

[11] N. Mishchuk, *J. Colloid Interface Sci.* **2008**, *320*, 599–607. https://doi.org/10.1016/j.jcis.2007.12.047

[12] J. Lützenkirchen, T. Preočanin, N. Kallay, *Phys. Chem. Chem. Phys.* **2008**, *10*, 4676. https://doi.org/10.1039/b812223g

[13] S. H. Cho, J. Y. Kim, J. H. Chun, J. D. Kim, *Colloids Surfaces A Physicochem. Eng. Asp.* **2005**, *269*, 28–34. https://doi.org/10.1016/j.colsurfa.2005.06.063

[14] R. Zimmermann, S. Dukhin, C. Werner, *J. Phys. Chem. B* **2001**, *105*, 8544–8549. https://doi.org/10.1021/jp004051u

[15] L. Kong, J. K. Beattie, R. J. Hunter, *J. Colloid Interface Sci.* **2001**, *238*, 70–79. https://doi.org/10.1006/jcis.2001.7464

[16] S. Usui, T. W. Healy, *J. Colloid Interface Sci.* **2001**, *240*, 127–132. https://doi.org/10.1006/jcis.2001.7661

[17] M. Manciu, E. Ruckenstein, *Colloids Surfaces A Physicochem. Eng. Asp.* **2012**, *400*, 27–35. https://doi.org/10.1016/j.colsurfa.2012.02.038

[18] J. K. Beattie, A. M. Djerdjev, *Angew. Chemie Int. Ed.* **2004**, 43, 3568–3571. https://doi.org/10.1002/anie.200453916

[19] M. Takahashi, *J. Phys. Chem. B* **2005**, 109, 21858–21864. https://doi.org/10.1021/jp0445270

[20] T. Preočanin, F. Šupljika, M. Lovrak, J. Barun, N. Kallay, *Colloids Surfaces A Physicochem. Eng. Asp.* **2014**, *443*, 129. https://doi.org/10.1016/j.colsurfa.2013.11.002

[21] J. K. Beattie, A. M. Djerdjev, G. G. Warr, *Faraday Discuss.* **2009**, *141,* 31–39. https://doi.org/10.1039/B805266B

[22] A. Gray-Weale, *Chem. Phys. Lett.* **2009**, *241*, 22–24. https://doi.org/10.1016/j.cplett.2009.09.008

[23] B. Winter, M. Faubel, R. Vácha, P. Jungwirth, *Chem. Phys. Lett.* **2009**, 474, 241–247. https://doi.org/10.1016/j.cplett.2009.04.053

[24] T. L. Tarbuck, S. T. Ota, G. L. Richmond, *J. Am. Chem. Soc.* **2006**, *128*, 14519–14527. https://doi.org/10.1021/ja063184b

[25] M. Mucha, T. Frigato, L. M. Levering, H. C. Allen, D. J. Tobias, L. X. Dang, P. Jungwirth, *J. Phys. Chem. B* **2005,** *109***,** 7617–7623. https://doi.org/10.1021/jp0445730

[26] R. Vácha, V. Buch, A. Milet, J. P. Devlin, P. Jungwirth, *Phys. Chem. Chem. Phys.* **2007**, 9, 4736. https://doi.org/10.1039/b704491g

[27] T. Preočanin, A. Selmani, P. Lindqvist-Reis, F. Heberling, N. Kallay, J. Lützenkirchen, *Colloids Surfaces A Physicochem. Eng. Asp.* **2012**, *412*, 120–128. https://doi.org/10.1016/j.colsurfa.2012.07.025

[28] W. Rudzinski, R. Charmas, J. M. Cases, M. Francois, F. Villieras, L. J. Michot, *Langmuir* **1997**, *13*,483. https://doi.org/10.1021/la960649a

[29] N. Kallay, T. Preočanin, S. Žalac, *Langmuir* **2004**, *20*, 2986–2988. https://doi.org/10.1021/la036185f

[30] A. Barišić, J. Lützenkirchen, G. Lefévre, T. Begović, *Colloids Surfaces A Physicochem. Eng. Asp.* **2019**, *579*, 123616. https://doi.org/10.1016/j.colsurfa.2019.123616

[31] N. Kallay, T. Preočanin, A. Selmani, D. Kovačević, J. Lützenkirchen, H. Nakahara, O. Shibata, *J. Phys. Chem. C* **2015**, *119*, 997–1007. https://doi.org/10.1021/jp507477u

[32] W. B. Holzapfel, *J. Chem. Phys.* **1969**, *50*, 4424–4428. https://doi.org/10.1063/1.1670914

[33] N. Kallay, T. Preočanin, D. Kovačević, J. Lützenkirchen, E. Chibowski, *Croat. Chem. Acta* **2010**, *83*, 357–370.

[34] T. Klačić, M. Tomić, D. Namjesnik, B. Pielić, T. Begović, *Environ. Chem.* **2019**, *16*, 529. https://doi.org/10.1071/EN19013

[35] T. Preočanin, N. Kallay, *Adsorption* **2013**, *19*, 259–267. https://doi.org/10.1007/s10450-012-9448-5

[36] J. N. Noh, J. A. Schwarz, *J. Colloid Interface Sci.* **1989**, *130*, 157–164. https://doi.org/10.1016/0021-9797(89)90086-6

[37] W. J. Wnek, R. Davies, *J. Colloid Interface Sci.* **1977**, *60*, 361–375. https://doi.org/10.1016/0021-9797(77)90295-8

[38] J. J. Carlson, S. K. Kawatra, *Miner. Process. Extr. Metall. Rev.* **2013**, *34*, 269–303. https://doi.org/10.1080/08827508.2011.604697

[39] Z. Brkljača, D. Namjesnik, J. Lützenkirchen, M. Předota, T. Preočanin, *J. Phys. Chem. C* **2018**, *122*, 24025–24036. https://doi.org/10.1021/acs.jpcc.8b04035

[40] N. Kallay, F. Šupljika, T. Preočanin, *Adsorption* **2013**, *19*, 211. https://doi.org/10.1007/s10450-012-9442-y

[41] A. Barišić, J. Lützenkirchen, N. Bebić, Q. Li, K. Hanna, A. Shchukarev, T. Begović, Experimental Data Contributing to the Elusive Surface Charge of Inert Materials in Contact with Aqueous Media. *Colloids Interfaces* **2021**, *5*, 6. https://doi.org/10.3390/colloids5010006

[42] G. Meraj, A. Chaudhari, *J. Mol. Liq.* **2014**, *190*, 1–5. https://doi.org/10.1016/j.molliq.2013.10.006

[43] M. Welborn, J. Chen, L. Wang, T. Van Voorhis, *J. Comput. Chem.* **2015**, *36*,934–939. https://doi.org/10.1002/jcc.23887

[44] A. Kakizaki, H. Motegi, T. Yoshikawa, T. Takayanagi, M. Shiga, M. Tachikawa, *J. Mol. Struct. THEOCHEM* **2009**, *901*, 1–8. https://doi.org/10.1016/j.theochem.2009.01.022

[45] G. Kovačević, T. Hrenar, N. Došlić, *Chem. Phys.* **2009**, *293*, 41–52. https://doi.org/10.1016/S0301-0104(03)00287-8

[46] T. Hrenar, ***qcc***, *Quantum Chemistry Code* (rev. 0.6826), Zagreb, Croatia, **2024.**

[47] I. Primožič, T. Hrenar, K. Baumann, L. Krišto, I. Križić, S. Tomić, *Croat. Chem. Acta* **2014**, *87*, 153. https://doi.org/10.5562/cca2476

[48] T. Hrenar, ***moonee***, *Code for Manipulation and Analysis of Multi- and Univariate Big Data* (rev. 0.68268), Zagreb, Croatia, **2024**

[49] J. Parlov Vuković, T. Hrenar, P. Novak, M. Friedrich, J. Plavec, *Energy Fuels* **2017**, *31*, 8095–8101. https://doi.org/10.1021/acs.energyfuels.7b01358